Supplementary Information

Novel robotic interface to evaluate, enable, and train locomotion and balance after neuromotor disorders

Nadia Dominici, Urs Keller, Heike Vallery, Lucia Friedli, Rubia van den Brand, Michelle L. Starkey, Pavel Musienko, Robert Riener and Grégoire Courtine

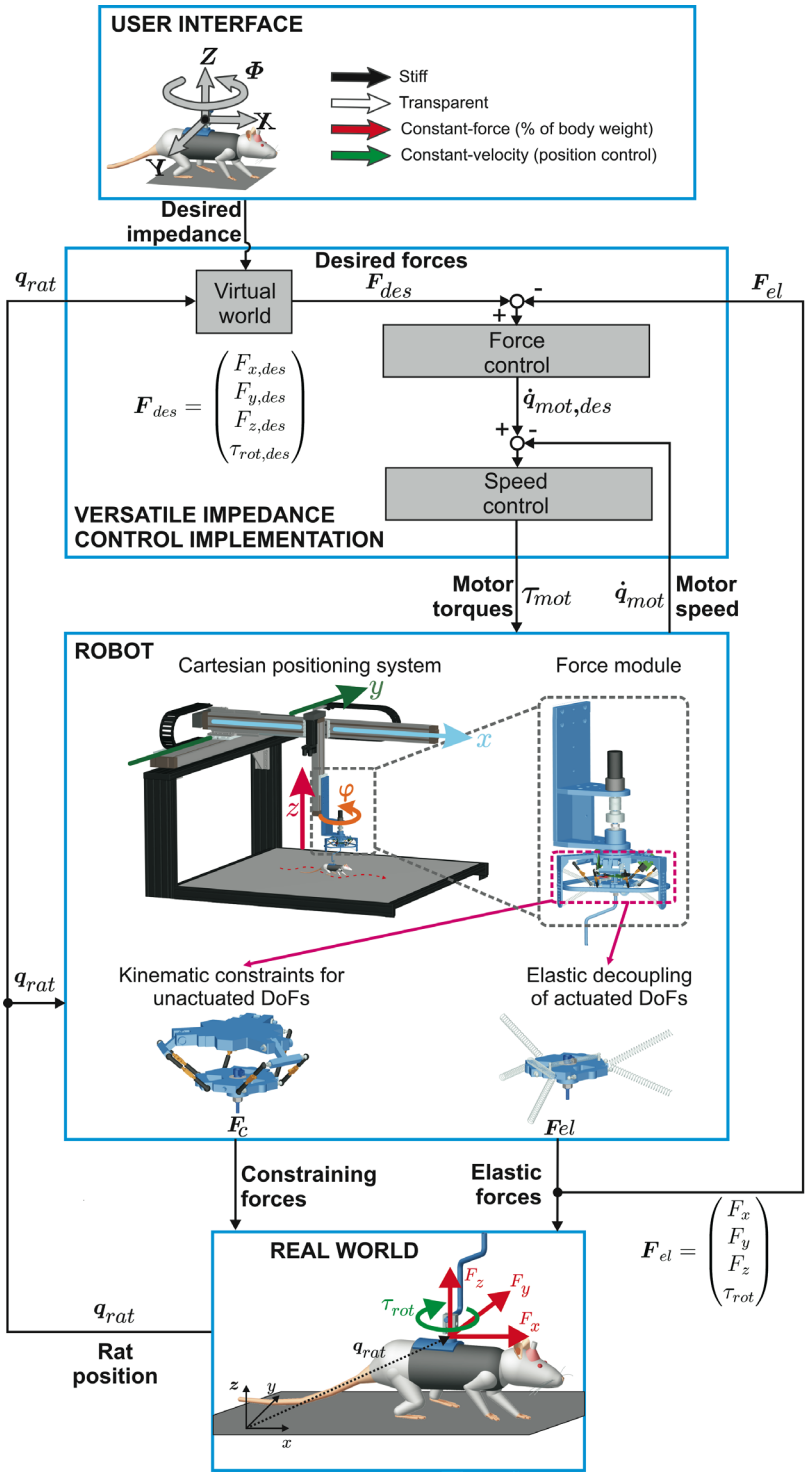

Supplementary Figure 1:Technical description of the robotic interface and control schemes

Supplementary Figure 1: Technical description of the robotic interface and control schemes

USER INTERFACE
A user-friendly GUI (Graphical user interface) is implemented in MATLAB/Simulink (The MathWorks, CA). The interface allows the user to create a virtual environment in which the applied forces or the end-effector position can be adjusted for each single actuated DoF of the robot. For example, the user can independently set any of the 4 actuated axes to behave transparently. Concomitantly, the other axes can provide a constant force that is proportional to the rat's body weight, as for supporting the rat against gravity. The axes can also be configured to be stiff in order to prevent lateral fall or to guide the rat along a user-defined trajectory. Alternatively, the user can control the displacement of the end-effector (position control), as for pushing the rat in a given direction, or along a user-defined trajectory. Finally, the user can introduce sudden changes in the virtual environment. For example, a user-defined perturbation can be superimposed onto any control scheme based on external triggers or the position of the rat in the real world. The different control strategies for the various locomotor paradigms can be found in **Supplementary Figure 2**.

VERSATILE IMPEDANCE CONTROL IMPLEMENTATION
We implemented an impedance control scheme that can adjust the force exerted by each actuated DoF of the robotic interface independently in real-time (1kHz). The controller is cascaded: an outer loop processes the position of the rat with respect to the virtual environment; for example a world with guiding walls or gravity-reduced conditions. This algorithm translates the virtual environment defined by the user into a vector $\boldsymbol{F}_{\text{des}}$ of desired forces. A force controller adjusts the desired motor speeds $\dot{\boldsymbol{q}}_{\text{mot,des}}$ sent to the drives based upon the error between the desired forces and the forces measured through spring deflection. An inner speed controller ensures that the actual motor speed $\dot{\boldsymbol{q}}_{\text{mot}}$ tracks the desired motor speed by commanding appropriate actuator torques τ_{mot}. The outer loops run on a Matlab xpc real-time operating system. The speed control runs on the actuator drives.

ROBOT
Cartesian positioning system: The robot consists of an actuated Cartesian positioning system that allows translations of the rat in the horizontal plane (x,y) while providing vertical support (z). An additional motor at the end-effector of this serial structure actuates rotation (φ). This serial configuration provides a large workspace in which forces can be applied to the animal in 4 DoFs.

Force module: To hide the inertia of the massive positioning robot and to measure the extremely small interaction forces between the robot and the rat, we developed a novel force module based on a "Series Elastic Actuator" (SEA). A SEA is composed of an actuator that is complemented with a passive compliant element in series. This compliance improves force control performance and effectively decouples actuator inertia to achieve a transparent interface. In the force module, we extended this SEA concept to 4 DoFs by providing multidimensional compliance at the end-effector of the positioning system.

Kinematic constraints for unactuated DoF: A mechanical "Delta" linkage prevents the rat from tilting in the 2 unactuated DoF, leading to constraining forces $\boldsymbol{F}_{\text{c}}$. The Delta structure also provides the means of measuring the end-effector position (rat position $\boldsymbol{q}_{\text{rat}}$) and subsequently the interaction forces $\boldsymbol{F}_{\text{el}}$ between the robot and the rat.

Elastic decoupling of actuated DoF: The compliance for the residual DoFs is achieved by multiple linear springs attached to the suspended platform and by an additional spring pair attached to the rotating shaft within the platform.

REAL WORLD
The rat is positioned in a custom-made, skin-like jacket made of light fabrics. A Velcro strip allows attachment of the rat onto a back plate with a rigid bar coming from the robot end-effector. The rat's position and the interaction forces with the robot are fed back to the impedance controller.

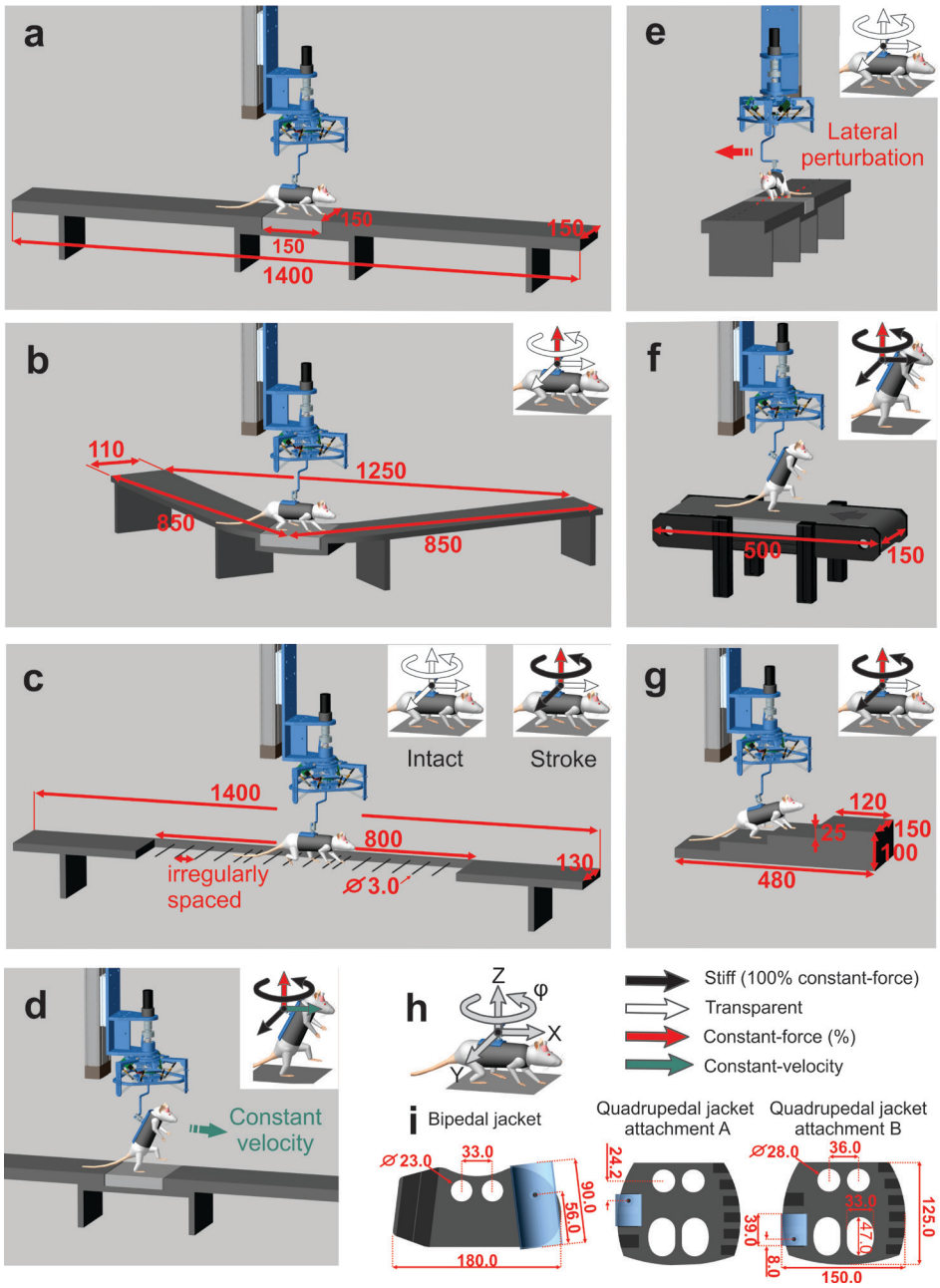

Supplementary Figure 2: Technical description of the locomotor testing paradigms
Locomotor capacities of intact and motor impaired rats were evaluated in a total of 7 tasks. **a.** Quadrupedal locomotion along a straight horizontal runway. **b.** Quadrupedal locomotion along a 90deg-curved horizontal runway. **c.** Quadrupedal locomotion along a straight horizontal ladder with irregularly spaced rungs. **d.** Bipedal locomotion along a straight horizontal runway. In this task, the robot propelled the rat forward at a constant velocity. **e.** Lateral perturbation (1s, 2.5N) introduced during continuous quadrupedal locomotion along a straight horizontal runway (task a). **f.** Continuous bipedal locomotion on a motorized treadmill belt. **g.** Quadrupedal locomotion along regularly spaced steps on a staircase. The various runways, stairs and ladders were made of wood but the walking surface was covered with turf to ensure a solid paw contact. The light grey box indicates the position of the force plate that measured ground reaction forces and ground reaction torques in X, Y, Z directions. **h.** For each task, the degree of compliance was adjusted for each translational and rotational axis independently. Control strategies included: stiff control (black), zero-force control (light grey, constant-force set to 0%), adjustable constant-force (red, constant-force set to a percentage of body weight), and constant-velocity (green, position control). The behavior of each axis in each task is reported in the upper corner of each panel. **i.** Features and dimensions of the various jackets. The Velcro pads are represented in dark. The position and size of the back attachment is shown in blue. All the dimensions are reported in mm.

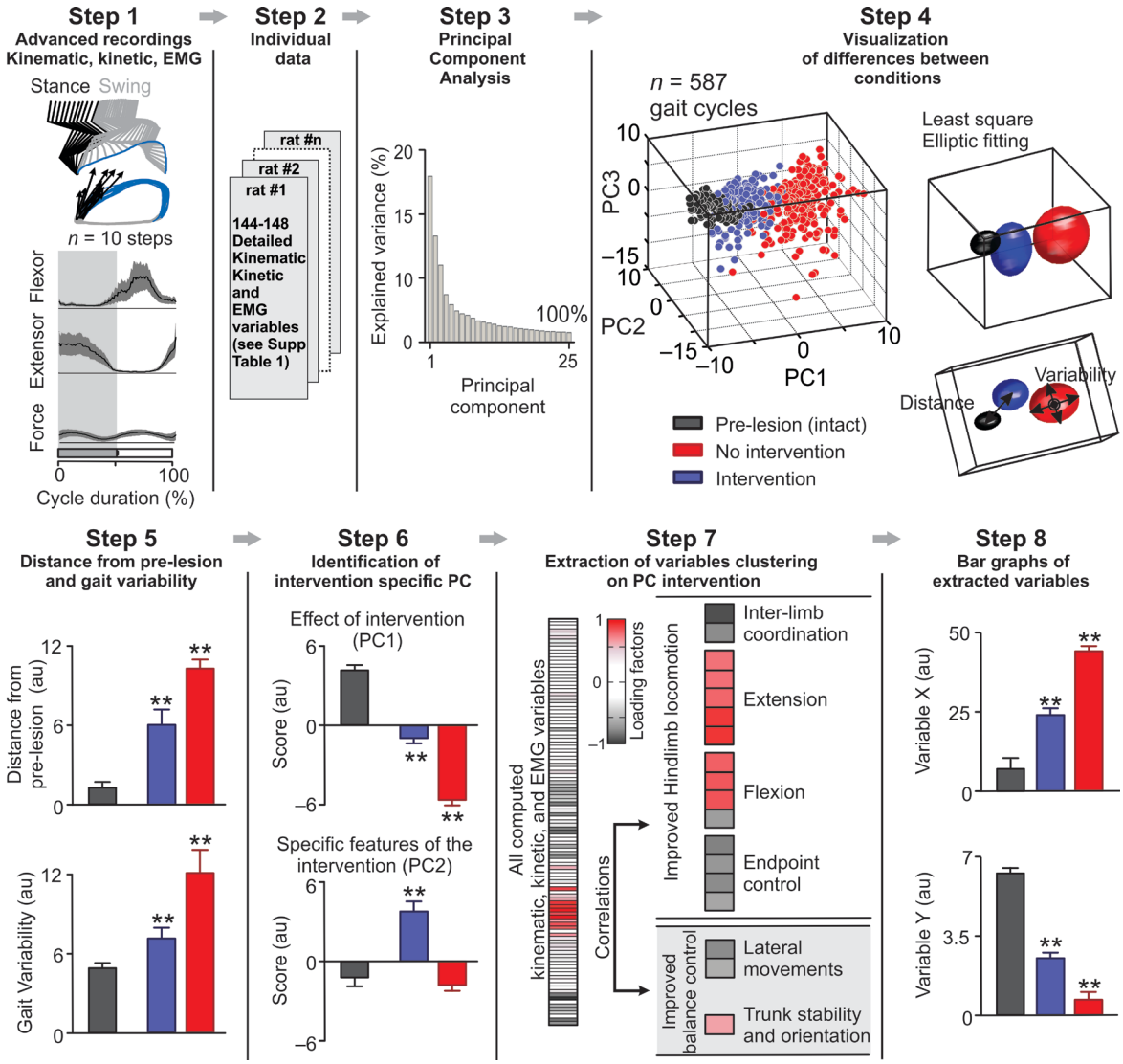

Supplementary Figure 3: Multi-step statistical analysis of gait parameters

We used a set of experimental data from our database to exemplify the multi-step statistical analysis that was applied for all the experiments described in this study. **Step1:** For all the experimental conditions, we collected kinematic, kinetic and EMG data during continuous locomotion using an advanced recording system**. Step 2:** We computed a large number of parameters that provides a comprehensive quantification of gait features. The complete list of computed parameters can be found in **Supplementary Table 1**. The analytic procedures and computations are detailed in Ref [1,2]. **Step 3:** We applied a principal component (PC) analysis on all the variables computed from all the gait cycles from all the rats and experimental conditions. This analysis constructs new variables, i.e. PC, that linearly combines the original variables and maximizes the amount of explained variance for each successive PC. Due to the high degree of correlation between gait parameters during locomotion, a few PCs are sufficient to explain a large proportion of the variance. **Step 4:** The gait cycles can be represented in the new "denoised" space created by PC1-3. In the proposed example, data points associated with each experimental condition cluster in a well-defined location, indicating that the rats exhibited intervention-specific gait patterns. Typically, PC1 differentiated gait cycles from intact rats (or pre-lesion), altered gaits from rats with SCI or stroke, and the improvement of locomotion with the robotic interface. In some instances, PC2 captured an additional feature. In the proposed example, PC2 is related to specific features of the intervention compared to intact and no intervention. In order to provide a straightforward representation of differences between conditions, we applied a least square elliptic fitting to the 3D data points. **Step 5:** To quantify the quality of gait performance, we measured the 3D geometric distance between the averaged location of gait cycles from each rat in a given condition and the average location of all gait cycles from all intact (or pre-lesion) rats. For each rat and condition, we also measured the 3D dispersion of gait cycles to provide a measure of gait variability. au, arbitrary unit. **Step 6:** The scores

(position of gait cycles in the PC space) reveal which conditions are differentiated along each PC. **Step 7:** We then extracted the factor loadings, i.e. correlation between each variable and each PC. We selected the PC of interest based upon step 6, and regrouped the variables with the highest factor loading (|value|> 0.5, $p < 0.05$) into functional clusters, which we named for clarity. Variables that load on the same PC correlate with each other. For instance, in the proposed example, improvement of hindlimb locomotion directly correlates with improved postural control. **Step 8:** To provide a more classic representation of differences between conditions, we generated histogram plots for one variable per extracted functional cluster.

References

1. Courtine, G.*, et al.*Transformation of nonfunctional spinal circuits into functional states after the loss of brain input. *Nat Neurosci* 12, 1333-1342 (2009).

2. Musienko, P.*, et al.* Controlling Specific Locomotor Behaviors through Multidimensional Monoaminergic Modulation of Spinal Circuitries. *J Neurosci* 31, 9264-9278 (2011).

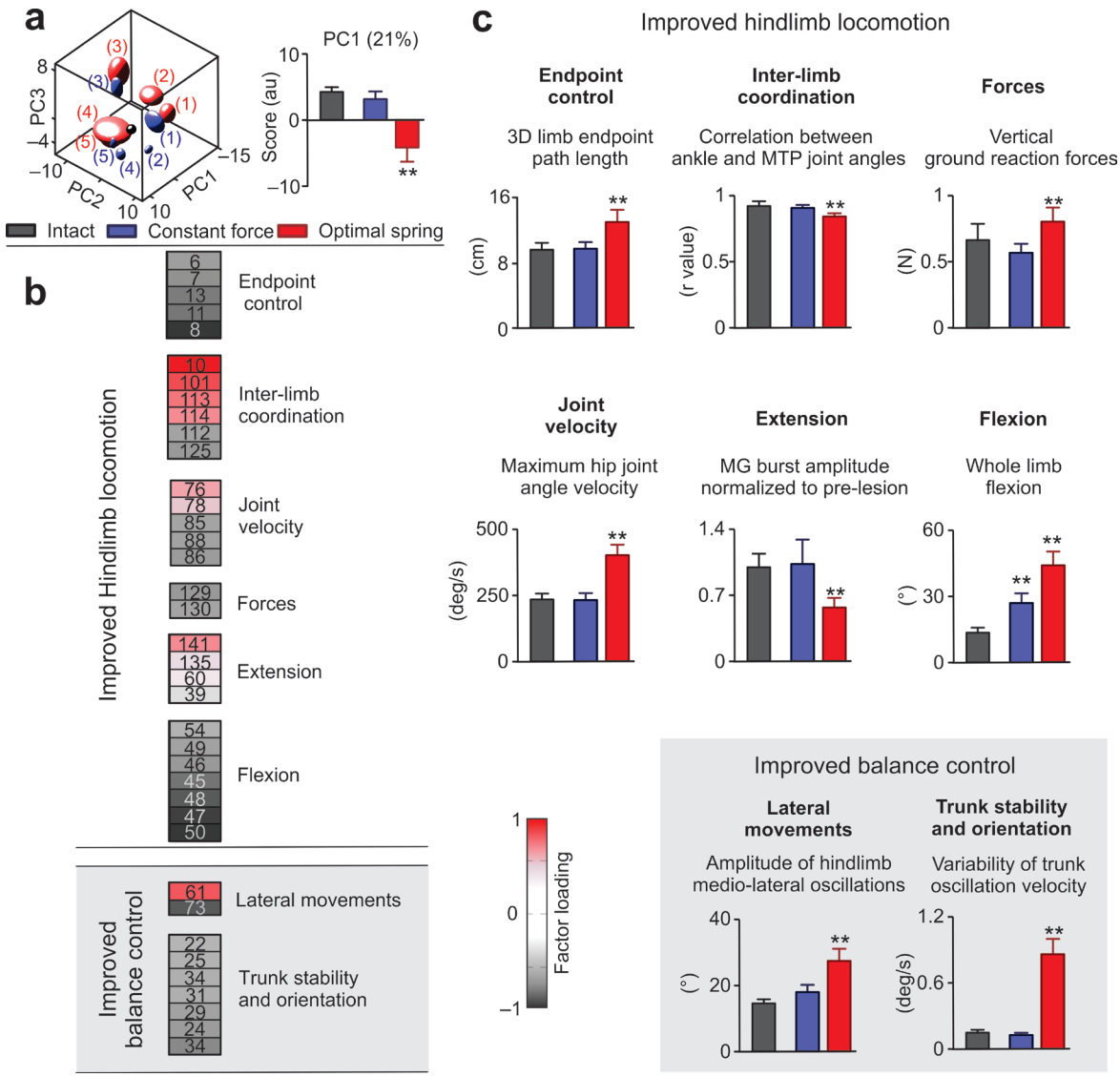

Supplementary Figure 4: Constant-force support leads to improved locomotor performance compared to spring-like support in rats with complete SCI

a. PC analysis (explained variance, 48%) applied on all gait cycles and rats (n = 10 per rat and per condition). Least square fitting was performed and indexed for each rat independently. The histogram plot reports mean values (n = 5 rats) of scores on PC1 for gait cycles recorded in intact rats and in spinal rats stepping with the same level of spring-like vs. constant force vertical support. au, arbitrary unit. **b.** Variables (numbers refer to **Supplementary Table 1**) with the highest factor loadings on PC1 (|value|> 0.5, $p < 0.05$) were regrouped in functional clusters. **c.** Histogram plots report mean values (n = 5 rats) for one variable per functional cluster for intact rats and spinal rats stepping with spring-like vs. constant force vertical support. **, significantly different from intact at $p < 0.05$.Error bars, S.E.M.

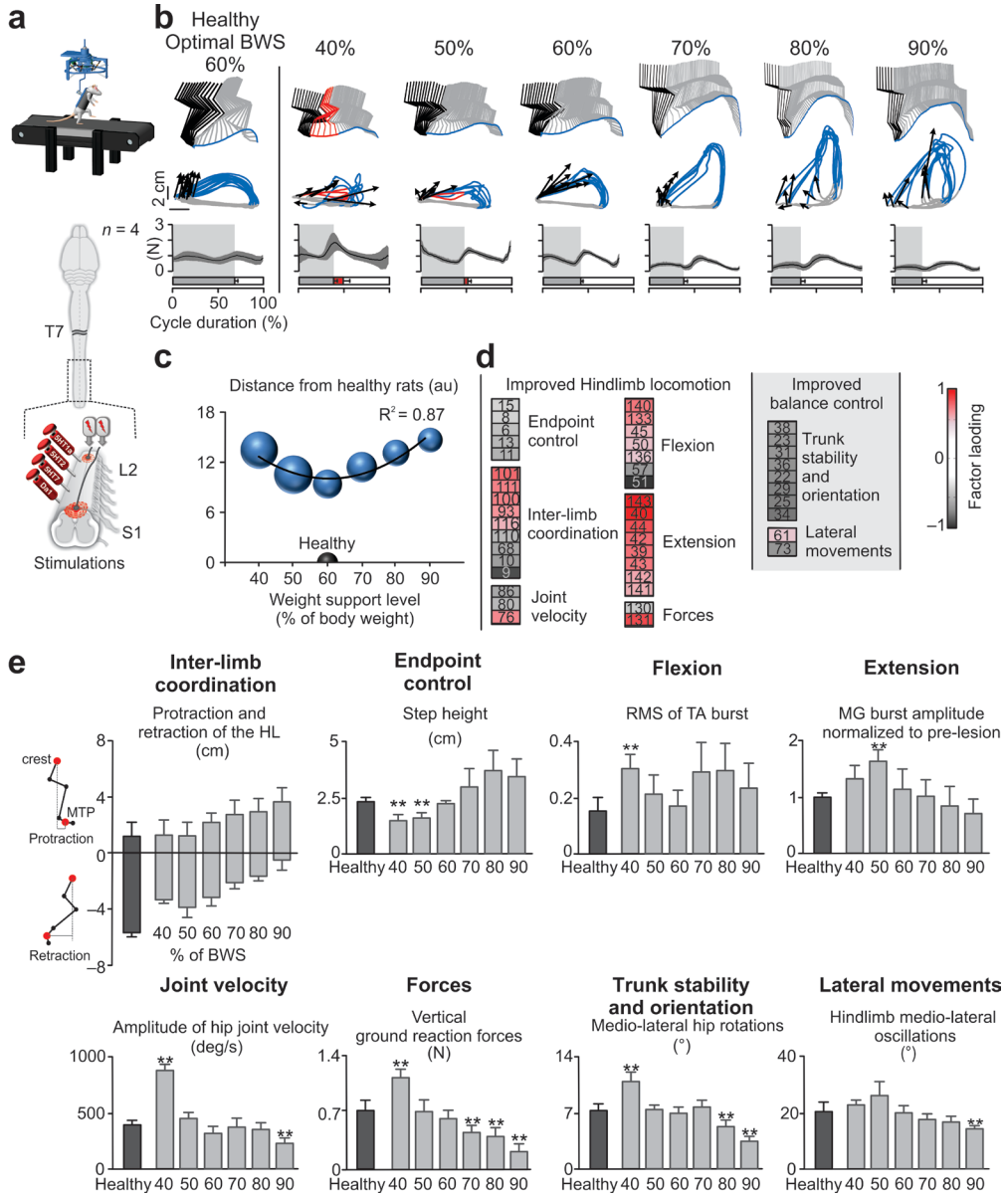

Supplementary Figure 5: Evaluation of the impact of weight bearing conditions on motor pattern generation in rats with complete SCI

a. Rats (n = 4 rats) received a complete SCI. After 5 weeks of recovery, the rats received enabling factors to encourage bipedal locomotion on a treadmill (13 cm.s-1). 10 gait cycles were recorded for each level of constant-force BWS (40-90%). Locomotion was recorded in healthy rats (n = 5) at 60% of BWS, which is the weight normally carried by the hindlimbs during quadrupedal gait**. b.** Representative stick diagram decomposition of hindlimb motion during stance (black), dragging (red), and swing (light grey) for each level of BWS, as well as for an intact rat. Successive color-coded trajectories of the hindlimb endpoint (n = 10 steps) are shown together with the orientation and intensity of the foot velocity vector (arrow) at swing onset. The average (n = 10 steps, +/- S.D.) vertical ground reaction forces (left and right hindlimbs combined) and relative duration of the stance (filled box), swing (open box), and drag (red) phases of gait are displayed at the bottom. **c.** Relationship between the level of BWS and the degree of gait pattern similarity compared to healthy rats (grey hemi-sphere), measured as the 3D distance from gait cycles in the PC analysis. The size of the spheres is proportional to gait variability, measured as the dispersion of each cluster in the PC analysis (See **Supplementary Figure 3**). A second-order polynomial fitting was applied to the data points to highlight the U-shaped relationship between stepping quality and BWS levels. au, arbitrary unit. **d.** Variables (numbers refer to **Supplementary Table 1**) with the highest factor loadings on PC1 (|value| > 0.5, $p < 0.05$) were regrouped in functional clusters. **e.** Histogram plots report mean values (n = 4 rats; error bar, S.E.M.) for one variable per functional cluster under the different levels of BWS. **, significantly different from intact at $p < 0.05$. Error bars, S.E.M.

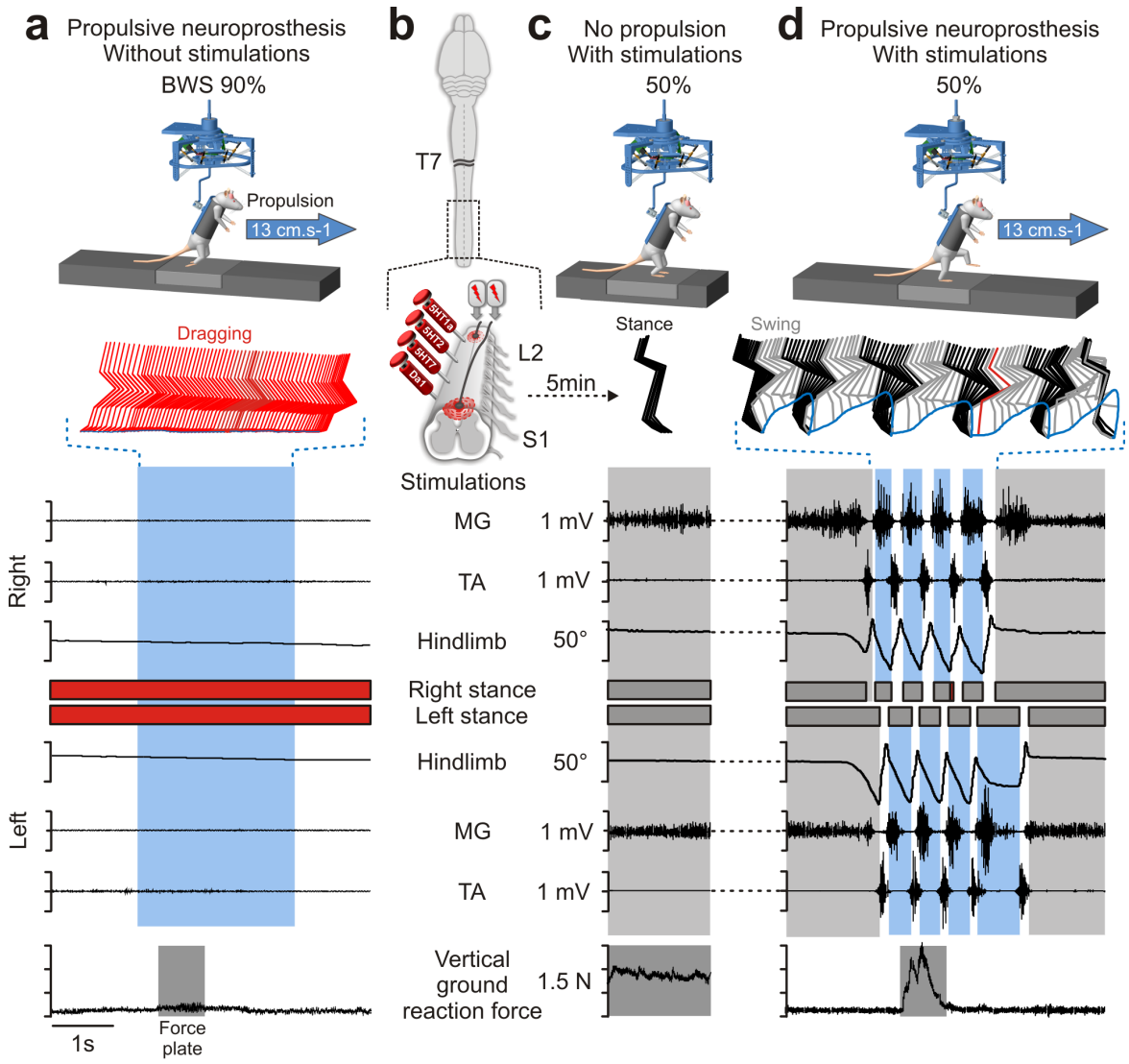

Supplementary Figure 6: The robotic propulsive neuroprosthesis enables coordinated overground locomotion in spinal rats

a. Spinal rats were positioned bipedally in the robotic interface. The robot was configured to move the body forward at a constant velocity (13 cm.s–1) while providing constant-force vertical support. Below the stick diagram decomposition of hindlimb motion and limb endpoint trajectories, the traces show angular oscillations of both hindlimbs, EMG activity of left and right MG and TA muscles, and vertical forces during a representative trial performed without stimulations. **b.** To enable hindlimb locomotion, rats received tonic epidural electrical stimulation at spinal segments S1 and L2, as well as a combination of agonists to 5HT1A, 5HT2A/C, 5HT7, and DA1-like receptors. **c.** With these stimulations, the spinal rats displayed tonic activity in left and right extensor muscles, and could stand for extensive periods of time. **d.** The animals immediately exhibited coordinated plantar stepping with alternation between both hindlimbs when the robot translated the trunk in the forward direction to replace the lost propulsive capacities.

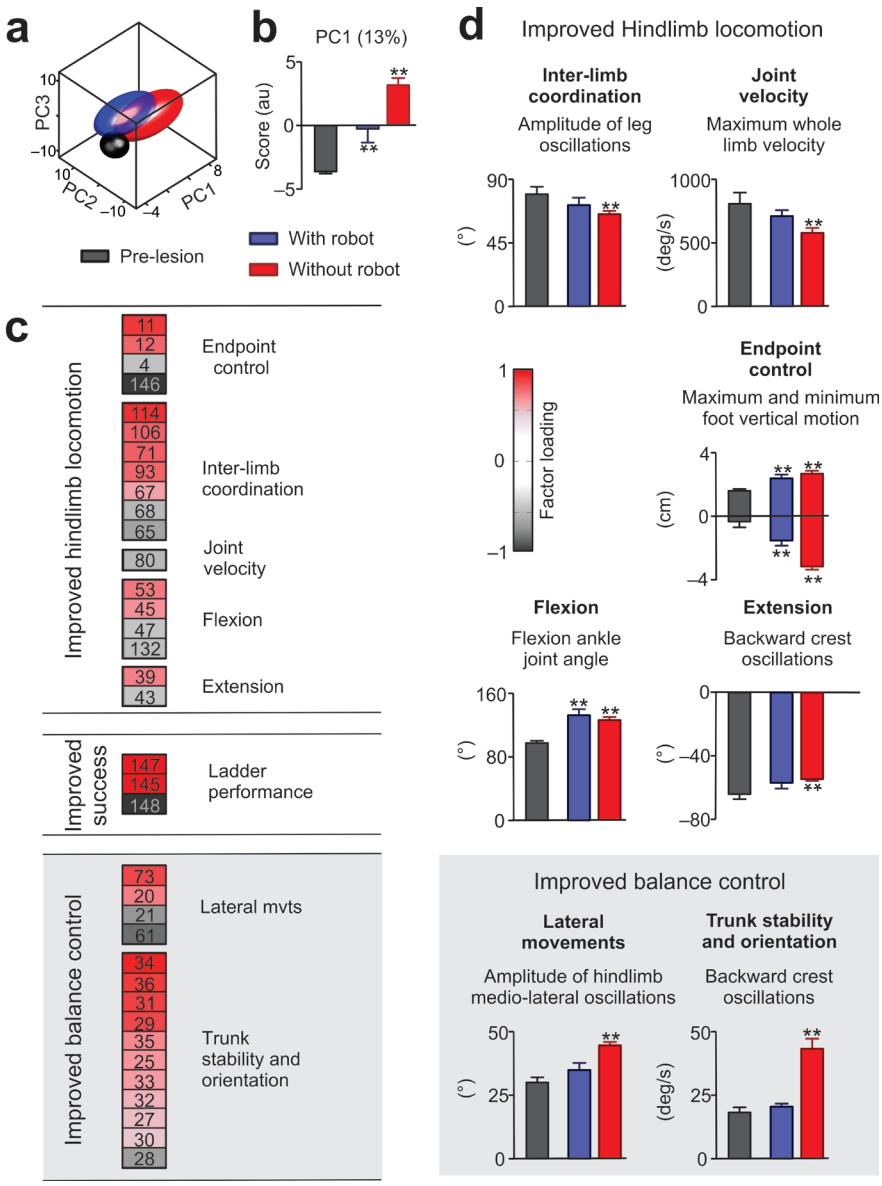

Supplementary Figure 7: Improved balance control with the postural neuroprosthesis correlates with improved hindlimb locomotion and performance during locomotion along a ladder with irregularly spaced rungs in rats with a cortical stroke

a. PC analysis was applied on all gait cycles recorded along the ladder in all the rats (n = 5) before and 2 days after lesion with and without vertical constant-force robotic support. Accurate and missed steps were both included in this analysis, but undifferentiated in the plot to emphasize the contrast between the conditions with and without robot. au, arbitrary unit. **b.** The histogram plot reports the mean values (n = 5 rats) of scores on PC1. **c.** Variables (numbers refer to **Supplementary Table 1**) with the highest factor loadings on PC1 (|value|> 0.5, $p < 0.05$) were regrouped in functional clusters. **d.** Histogram plots report mean values (n = 5 rats) for one variable per functional cluster, except for the improved measures of success that are reported in **Figure 3b**. **, significantly different from intact at $p < 0.05$. Error bar, S.E.M.

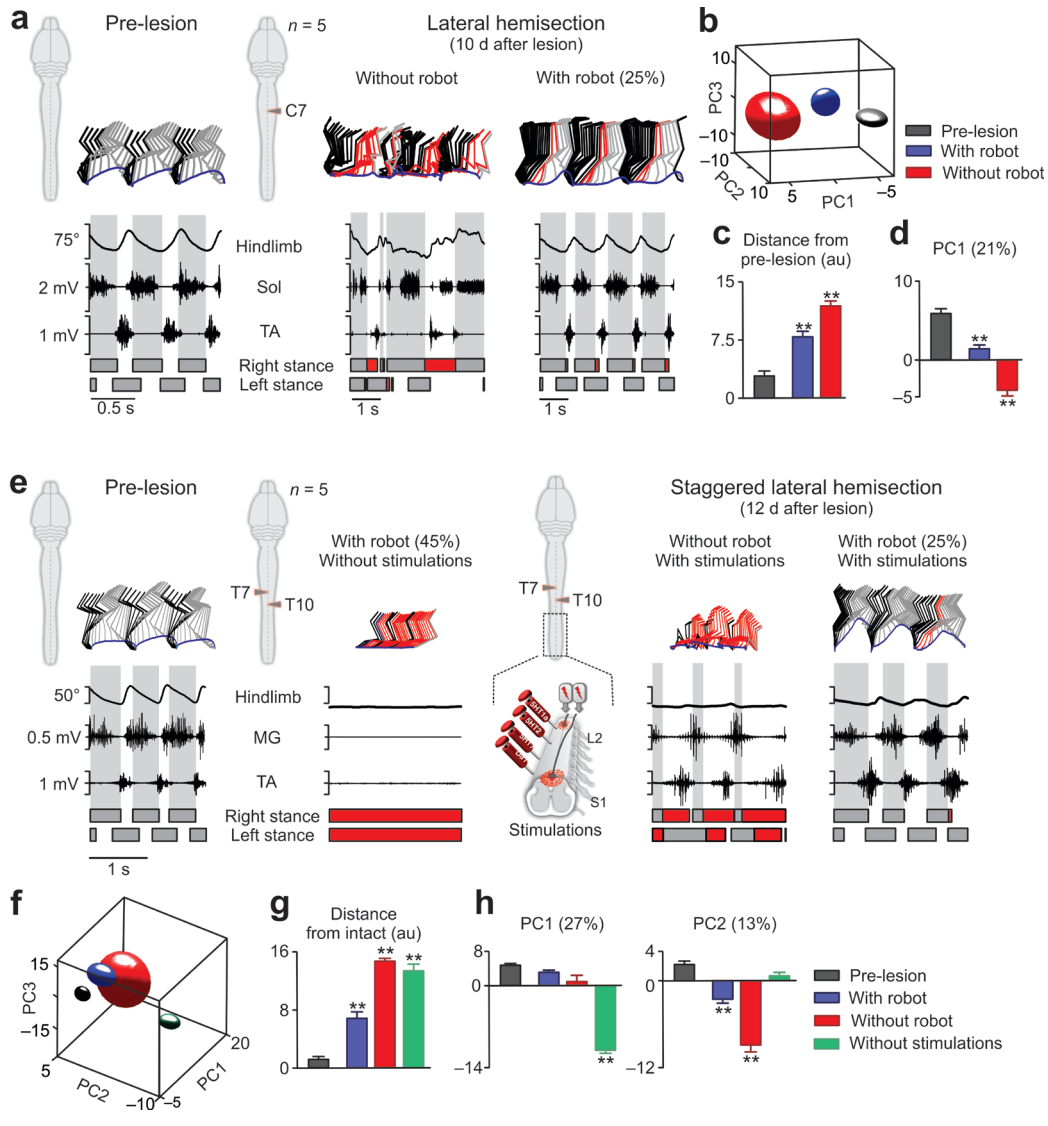

Supplementary Figure 8: Improved balance control with the postural neuroprosthesis correlates with improved hindlimb locomotion during straight horizontal runway locomotion in rats with moderate and severe SCI

a. Stick diagram decomposition of hindlimb motion, hindlimb oscillations, and EMG activity of Sol and TA muscles recorded pre-lesion as well as 10 days after a lateral cervical (C7) hemisection with and without constant-force robotic support. **b.** PC analysis was applied on all gait cycles recorded in all the rats (n = 5) before and 10 days after lesion with and without robotic support. **c.** The histogram plot reports mean values (n = 5 rats) of the 3D distance from the mean location of pre-lesion gaits in the PC space. **d.** PC1 scores. **e.** Hindlimb kinematics and EMG activity of MG and TA muscles recorded pre-lesion as well as 12 days after staggered lateral hemisections without enabling factors (no stimulations) as well as with stimulations without and with constant-force robotic support. **f.** PC analysis was applied on all gait cycles recorded in all the rats (n = 5) before and 10 days after lesion without stimulations as well as with and without robotic support. **g.** The histogram plot reports mean values (n = 5 rats) of the 3D distance between the different experimental conditions and the mean location of pre-lesion gaits in the PC space. **h.** PC1 differentiates actual stepping vs. paralysis, while PC2 highlights the improvement of locomotion with the postural neuroprosthesis. **, significantly different from intact at $p < 0.05$. au, arbitrary unit**.** Error bar, S.E.M.

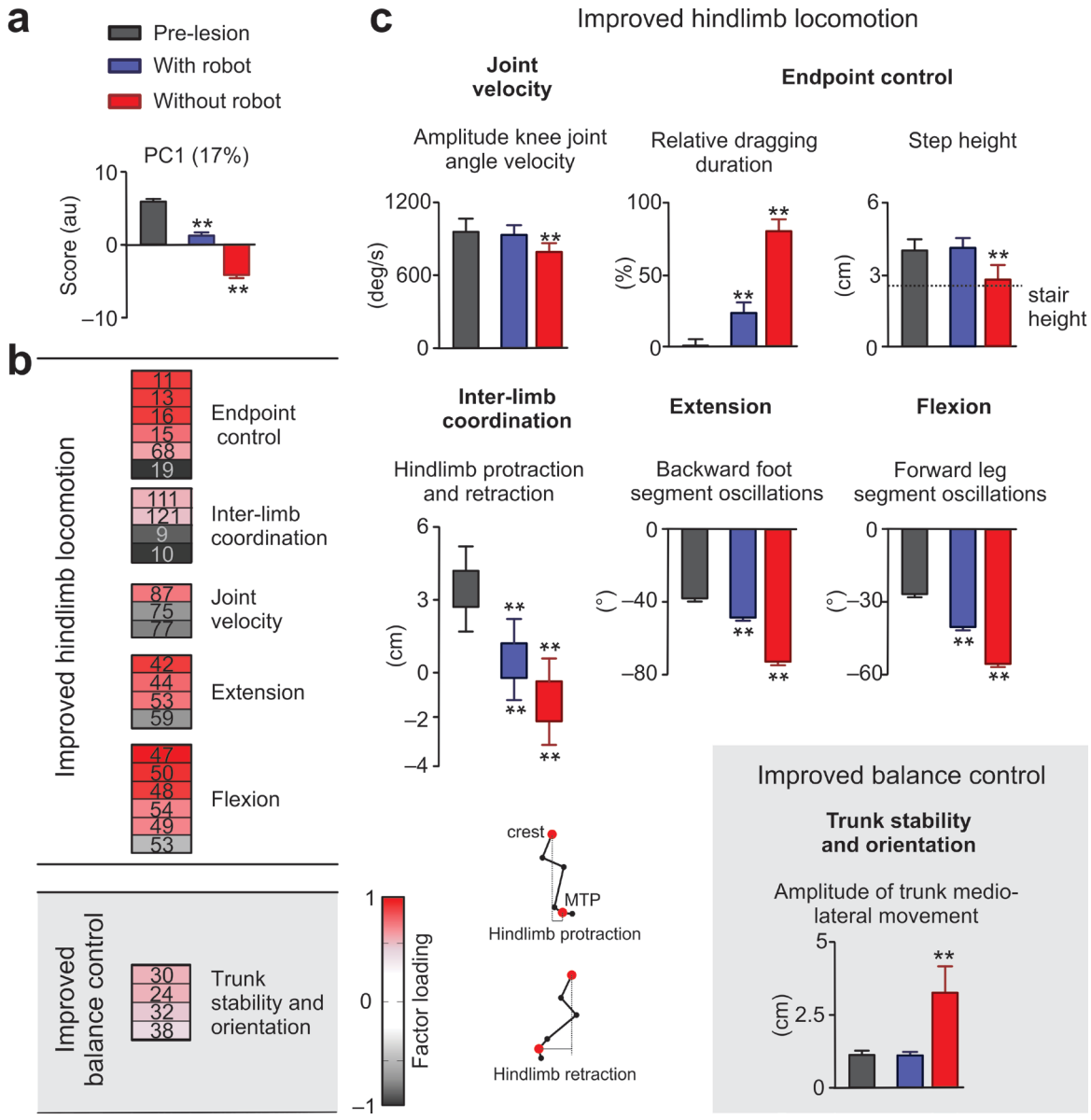

Supplementary Figure 9: Improved balance control with the postural neuroprosthesis correlates with improved hindlimb locomotion during locomotion on a staircase in rats with moderate SCI

a. Histogram plots report mean values (n = 5 rats) of scores on PC1 for gait cycles recorded before as well as 10 days after a lateral cervical (C7) hemisection without and with constant-force robotic support.au arbitrary unit. **b.** Variables (numbers refer to **Supplementary Table 1**) with the highest factor loadings on PC1 (|value|> 0.5, $p < 0.05$) were regrouped in functional clusters. **c.** Histogram plots report mean values (n = 5 rats) for one variable per functional cluster. **, significantly different from intact at $p < 0.05$.Error bar, S.E.M.

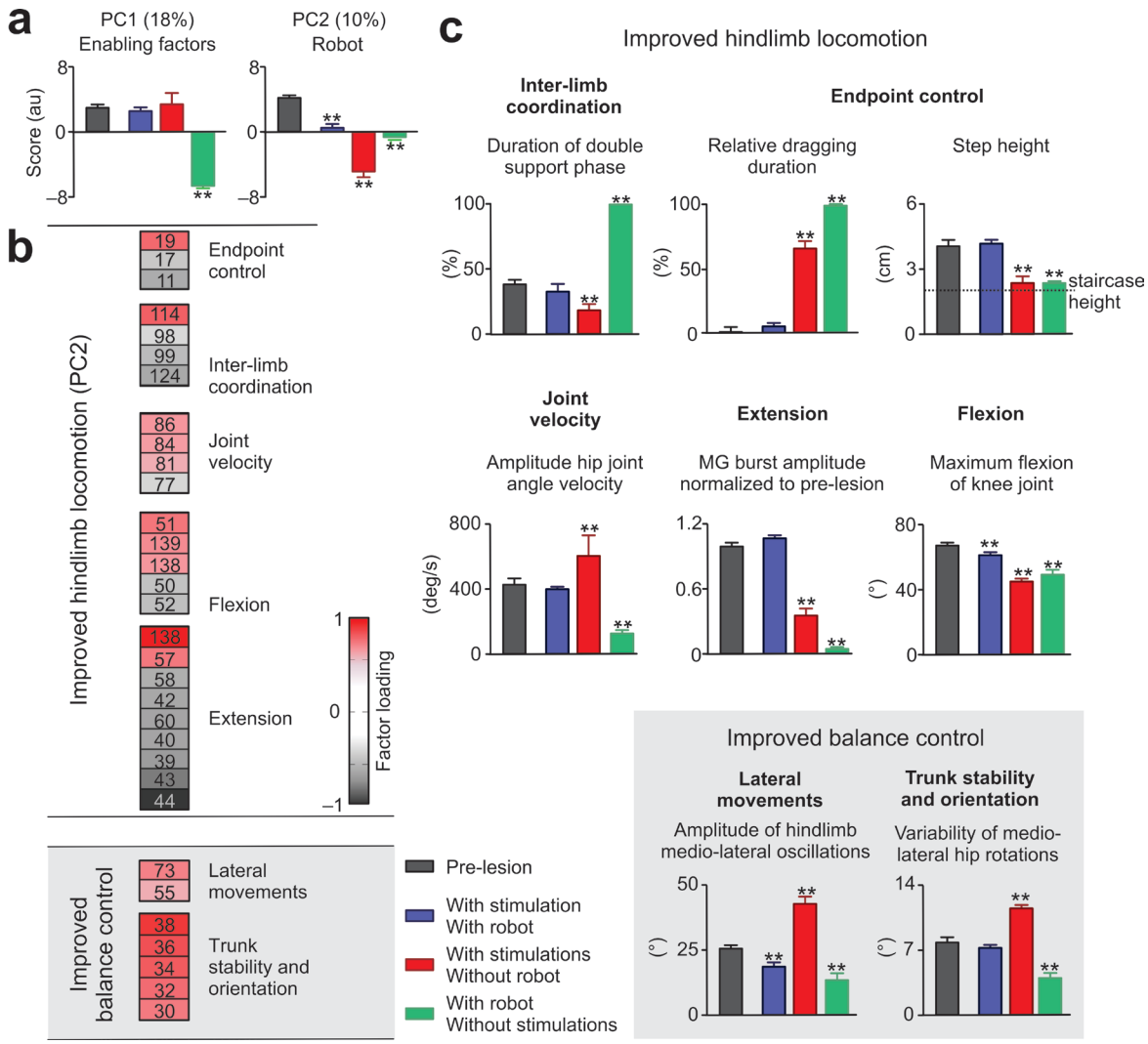

Supplementary Figure 10: Improved balance control with the postural neuroprosthesis correlates with improved hindlimb locomotion during locomotion on a staircase in rats with severe SCI

a. Histogram plots report mean values (n = 5 rats) of scores on PC1 and PC2 for gait cycles recorded before the lesion and 12 days after staggered lateral hemisections under the various experimental conditions. PC1 captures the effect of motor control enabling factors, which promoted hindlimb motion in otherwise paralyzed rats. PC2 captures the improvements of hindlimb locomotion and balance control with the robotic interface. au, arbitrary unit. **b.** Variables (numbers refer to **Supplementary Table 1**) with the highest factor loadings on PC2 (|value|> 0.5, $p < 0.05$) were regrouped in functional clusters. **c.** Histogram plots report mean values (n = 5 rats; error bar, S.E.M.) for one variable per functional cluster under the different experimental conditions. **, significantly different from intact at $p < 0.05$. error bar, S.E.M.

Supplementary Table 1. Computed Kinematics, Kinetics, and EMG Parameters of Gait Parameters

Parameters		#	Detailed explanation
Kinematics			
Temporal features of gait			
		1	Cycle velocity
		2	Cycle duration
		3	Stance duration
		4	Relative stance duration (percent of the cycle duration)
		5	Swing duration
Limb endpoint (MTP) trajectory			
		6	Stride length
		7	Step length
		8	3D limb endpoint path length
		9	Maximum backward position
		10	Minimum forward position
		11	Step height
		12	Relative position of main peak
		13	Maximum speed during swing
		14	Relative timing of maximum velocity during swing
		15	Acceleration at swing onset
		16	Endpoint velocity
		17	Orientation of the velocity vector at swing onset
		18	Dragging
		19	Relative dragging duration (percent of swing duration)
Stability			
Base of support		20	Positioning of the foot at stance onset with respect to the pelvis
		21	Stance width
Trunk and pelvic position and oscillations		22	Variability of sagittal trunk oscillations
		23	Variability in velocity of sagittal trunk oscillations
		24	Variability of Medio-lateral hip oscillations
		25	Variability of vertical mid-point hip oscillations
		26	Variability of Medio-lateral mid-point shoulder oscillations
		27	Variability of vertical mid-point shoulder oscillations
		28	Maximum trunk vertical position
		29	Amplitude of trunk vertical movement
		30	Amplitude of trunk Medio-lateral movement
		31	Variability of vertical trunk movement
		32	Variability of Medio-lateral trunk movement
		33	Variability of Medio-laterale trunk velocity
		34	Variability of vertical trunk velocity
		35	Variability of trunk acceleration in Medio-lateral direction
		36	Variability of trunk acceleration in vertical direction
		37	Variability of Medio-lateral shoulder rotations
		38	Variability of Medio-lateral hip rotations
Joint angles and segmental oscillations			
Backward	proximal	39	Crest oscillations
		40	Thigh oscillations
		41	Leg oscillations
		42	Foot oscillations
	distal	43	Toe oscillations
Forward	whole limb	44	Whole limb oscillations
	proximal	45	Crest oscillations
		46	Thigh oscillations
		47	Leg oscillations
		48	Foot oscillations
	distal	49	Toe oscillations
Flexion	whole limb	50	Whole limb oscillations
	proximal	51	Hip joint angle
		52	Knee joint angle
		53	Ankle joint angle
Abduction	distal	54	MTP joint angle
	whole limb	55	Whole limb abduction
	distal	56	Foot abduction
Extension	proximal	57	Hip joint angle
		58	Knee joint angle
		59	Ankle joint angle
Adduction	distal	60	MTP joint angle
	whole limb	61	Whole limb adduction
	distal	62	Foot adduction
Amplitude	proximal	63	Crest oscillations
		64	Thigh oscillations
		65	Leg oscillations
		66	Foot oscillations
	distal	67	Toe oscillations
	whole limb	68	Whole limb oscillations
	proximal	69	Hip joint angle
		70	Knee joint angle
		71	Ankle joint angle
	distal	72	MTP joint angle
	whole limb	73	Whole limb medio-lateral oscillations
	distal	74	Foot abduction /adduction

Parameters		#	Detailed explanation
Kinematics			
Velocity			
Minimum	whole limb	75	Whole limb oscillation velocity
	proximal	76	Hip joint angle velocity
		77	Knee joint angle velocity
		78	Ankle joint angle velocity
	distal	79	MTP joint angle velocity
Maximum	whole limb	80	Whole limb oscillation velocity
	proximal	81	Hip joint angle velocity
		82	Knee joint angle velocity
		83	Ankle joint angle velocity
	distal	84	MTP joint angle velocity
Amplitude	whole limb	85	Whole limb angle velocity
	proximal	86	Hip joint angle velocity
		87	Knee joint angle velocity
		88	Ankle joint angle velocity
	distal	89	MTP joint angle velocity
Inter-limb coordination			
PC analysis		90	Degree of linear coupling between joint oscillations
FFT decomposition	proximal	91	Temporal coupling between crest and thigh oscillations
		92	Temporal coupling between thigh and leg oscillations
		93	Temporal coupling between leg and foot oscillations
	distal	94	Temporal coupling between foot and toe oscillations
Cross-correlation	proximal	95	Correlation between crest and tight oscillations
		96	Correlation between tight and leg oscillations
		97	Correlation between leg and foot oscillations
	distal	98	Correlation between foot and toe oscillations
	proximal	99	Correlation between hip and knee oscillations
		100	Correlation between knee and ankle oscillations
	distal	101	Correlation between ankle and MTP oscillations
Relative coupling	proximal	102	Temporal lag between backward positions of crest and thigh oscillations
		103	Temporal lag between forward positions of crest and thigh oscillations
		104	Temporal lag between backward positions of thigh and leg oscillations
		105	Temporal lag between forward positions of the thigh and leg oscillations
		106	Temporal lag between backward positions of leg and foot oscillations
		107	Temporal lag between forward positions of leg and foot oscillations
		108	Temporal lag between backward positions of foot and toe oscillations
	distal	109	Temporal lag between forward positions of foot and toe oscillations
inter-segmental coordination		110	Percentage of variance (1th eigenvector) between segmental oscillations
		111	Percentage of variance (2th eigenvector) between segmental oscillations
		112	Percentage of variance (3th eigenvector) between segmental oscillations
		113	1th eigenvector (long axis of the gait-loop) projection on thigh axis
		114	1th eigenvector (long axis of the gait-loop) projection on shank axis
		115	1th eigenvector (long axis of the gait-loop) projection on foot axis
		116	2th eigenvector (short axis of the gait-loop) projection on thigh axis
		117	2th eigenvector (short axis of the gait-loop) projection on shank axis
		118	2th eigenvector (short axis of the gait-loop) projection on foot axis
		119	3th eigenvector (normal to the the gait-loop plane) projection on thigh axis
		120	3th eigenvector (normal to the the gait-loop plane) projection on shank axis
		121	3th eigenvector (normal to the the gait-loop plane) projection on foot axis
		122	Area of the gait-loop
Left-right hindlimb coordination		123	Ratio of left to right hindlimb cycle duration
		124	Double stance duration
		125	Correlation between whole hindlimb oscillations
Forelimb and hindlimb coordination		126	Correlation between hindlimb and ipsilateral forelimb oscillations
		127	Correlation between hindlimb and contralateral forelimb oscillations
Kinetics			
		128	Medio-lateral forces
		129	Anteroposterior forces
		130	Vertical forces
		131	Weight bearing level
EMG			
Timing (relative to cycle duration, paw contact to paw contact)			
Flexor		132	Relative onset of TA EMG burst
		133	Relative end of TA EMG burst
Extensor		134	Relative onset of MG/Sol EMG burst
		135	Relative end of MG/Sol EMG burst
Duration			
Flexor		136	TA EMG burst
Extensor		137	MG/Sol EMG burst
Amplitude			
Flexor		138	Mean amplitude of TA EMG burst
		139	Integral of TA EMG burst
		140	Root mean square of TA EMG burst
Extensor		141	Mean amplitude of MG/Sol EMG burst
		142	Integral of MG/Sol EMG burst
		143	Root mean square of MG EMG burst
Antagonist co-contraction			
		144	Co-contraction of MG/Sol and TA muscles
Ladder performance			
		145	Relative horizontal position of the foot-rung during stance
		146	Relative vertical position of the foot-rung during stance
		147	Relative horizontal position of the foot (percent distance between rungs)
		148	Performance score (0 Accurate; 1 Slip; 2 Miss)